eprints@whiterose.ac.uk
https://eprints.whiterose.ac.uk/

Dual-Continuum Design Approach for Intuitive and Low-Cost Upper Gastrointestinal Endoscopy

Nicolo Garbin[1], Long Wang[1], James H. Chandler[2], Keith L. Obstein[3,1], Nabil Simaan[1], Pietro Valdastri[2,1]

Abstract—**Objective: This paper introduces a methodology to design intuitive, low-cost, and portable devices for visual inspection of the upper gastrointestinal tract.**

Methods: The proposed approach mechanically couples a multi-backbone continuum structure, as the user interface, and a parallel bellows actuator, as the endoscopic tip. Analytical modeling techniques derived from continuum robotics were adopted to describe the endoscopic tip motion from user input, accounting for variations in component size and pneumatic compressibility. The modeling framework was used to improve intuitiveness of user-to-task mapping. This was assessed against a 1:1 target, while ease-of-use was validated using landmark identification tasks performed in a stomach simulator by one expert and ten non-expert users; benchmarked against conventional flexible endoscopy. Pre-clinical validation consisted of comparative trials in *in-vivo* porcine and human cadaver models.

Results: Target mapping was achieved with an average error of $5°$ in bending angle. Simulated endoscopies were performed by an expert user successfully, within a time comparable to conventional endoscopy (<1 minute difference). Non-experts using the proposed device achieved visualization of the stomach in a shorter time (9s faster on average) than with a conventional endoscope. The estimated cost is <10 USD and <30 USD for disposable and reusable parts, respectively.

Significance and Conclusions: Flexible endoscopes are complex and expensive devices, actuated via non-intuitive cable-driven mechanisms. They frequently break, requiring costly repair, and necessitate a dedicated reprocessing facility to prevent cross contamination. The proposed solution is portable, inexpensive, and easy to use, thus lending itself to disposable use by personnel without formal training in flexible endoscopy.

Index Terms—**disposable endoscopy, parallel bellows actuator, multi-backbone manipulator, intuitiveness, low cost, continuum robots.**

LIST OF ABBREVIATIONS

AGC - antrum greater curvature;

ALC - antrum lesser curvature;

BGC - body greater curvature;

BLC - body lesser curvature;

DAQ - data acquisition board;

DCE - dual-continuum endoscope;

DOF - degree of freedom;

EGD - esophagogastroduodenoscopy;

EM - electromagnetic;

ER - emergency room;

ET - endoscopic tip;

FE - flexible endoscope;

GEJ - gastroesophageal junction;

GI - gastrointestinal;

GP - general practitioner;

ICU - intensive care unit;

LED - light emitting diode;

MIS - minimally invasive surgery;

MP - mass production;

PBA - parallel bellows actuator;

RMSE - root mean squared error;

UGI - upper GI;

UI - user interface;

US - United States.

[1] Nicolo Garbin, Long Wang, Keith L. Obstein and Nabil Simaan are with the Department of Mechanical Engineering, Vanderbilt University, Nashville, TN 37212, USA. e-mail: (nicolo.garbin.1, long.wang, nabil.simaan)@vanderbilt.edu

[2] James H. Chandler and Pietro Valdastri are with the School of Electronic and Electrical Engineering, University of Leeds, Leeds, UK. e-mail: (J.H.Chandler, P.Valdastri)@leeds.ac.uk

[3] Keith L. Obstein is also with the Department of Gastroenterology, Hepatology, Nutrition, Vanderbilt University Medical Center, Nashville, TN 37212, USA. e-mail: keith.obstein@vanderbilt.edu

I. INTRODUCTION

Flexible endoscopes (FEs) are medical instruments used for the investigation of the gastrointestinal (GI) tract in a range of procedures that include Esophagogastroduodenoscopy (EGD) (i.e. examination of the upper gastro-intestinal (UGI) region). EGD is a very common procedure (>6.9 million EGDs per year in the US alone [1]), and is typically performed in a dedicated endoscopy suite due to the need for sedation, monitoring equipment, and trained personnel [2].

FE are complex, expensive, and non-intuitive medical devices that are cable actuated [3]. Most of the commercially available FEs are non-disposable and require reprocessing to avoid cross-contamination [4]. Despite reprocessing, FE related infections remain a concern and can lead to significant patient morbidity and mortality [5]. In addition, the durability of these devices is less than ideal, with breakage rates ranging from 1-10% at an average repair cost of 5,833 USD [6].

Among the indications that currently result in referral for an EGD, some may be over-served by the use of conventional FEs, and could benefit from a simpler, cheaper, and more hygienic solution. In particular, purely visual inspection (i.e. without biopsy sampling) may be appropriate for the vast majority of cases, with referral to full EGD if suspicious

lesions are identified [7]. A visualization device that is easy to use and disposable has the potential to allow healthcare personnel without a formal GI training or access to reprocessing facilities to perform visual inspection of the UGI tract. In [8], endoscopy-based triage was demonstrated to improve patients outcome and reduce hospital costs. This study also highlighted the need for a device that is easy enough to use without specialistic training. Such a device would expand the availability of UGI endoscopy to general practitioners (GP), mid-level providers, emergency room (ER) clinicians, and intensive care unit (ICU) personnel. If manufacturing costs are low, then such a device would also be extremely beneficial in underdeveloped settings (e.g. low-income countries or rural areas of middle-income countries) where UGI tract pathologies have a high incidence [9], but access to healthcare facilities is scarce (e.g. Central America, rural areas of China and India) and screening programs are currently too costly to implement [10].

Commercially available disposable endoscopes include colonoscopes (SC210, Invendo Medical GmbH, now Ambu A/S, Copenhagen, Denmark) [11], and magnetically controlled capsule endoscopes (NaviCam, Ankon Technologies Co, Ltd, Wuhan, China) [12]. However, these systems still require specialized locales to operate, and are targeted as a substitute for conventional FE, hence requiring conventionally trained operators. Conversely, a device that is supplementary in nature to conventional FE, while maintaining a lower cost, may have greater impact on the availability of UGI screening.

An example of a low-cost, disposable endoscopic platform for UGI cancer screening is the Hydrojet – a 10 mm diameter flexible catheter actuated via pressurized water jets located at the base of the distal viewing tip. The Hydrojet delivers a flexible and disposable endoscopic platform at <2 USD per case. However, significant challenges related to delivering intuitive and precise motion control of the viewing tip still remain to be addressed [13].

Continuum robots, defined as actuated structures whose constitutive materials form curves with continuous tangent vectors, have found numerous applications within surgical procedures [14], [15]. Examples include concentric tube robots/active cannulas [16], [17] and multi-backbone continuum robots [18], [19] for trans-oral upper airway surgery [20], single port access surgery [21], [22], minimally invasive surgery (MIS) [23], and arthroscopy [24].

The suitability, and therefore prevalence, of multi-backbone continuum medical devices may be attributed to their large range of motion, with the ability to provide high accuracy under telemanipulation guidance (e.g. [21] reported sub-millimetre motion accuracy during autonomous manipulation). However, these devices require active compliance control schemes to ensure safe insertion into human anatomy [25], thus increasing the complexity of clinical translation.

A safer implementation of the continuum approach is provided by soft, fluid driven, manipulators [26]. Examples under development for endoscopic applications are described in [27–29]. These are silicone molded devices that elongate and bend when their internal chambers are pressurized. Although these actuators can be fabricated at relatively low cost, the complexity of the material properties and internal structures provides non-linear responses, which are problematic for attaining accurate kinematic models and closed loop control. An approach that is more straightforward to model, yet maintains the benefit of having soft structures, consists in adopting expandable chambers in the form of bellows, mounted in a parallel configuration (parallel bellows actuator - PBA). A linear relationship between input pressure and bellows elongation has shown to be effective in predicting the system behaviour for closed loop control of PBA [30–32]. This approach has been extensively described in [33], [34] to control the bellows-actuated Bionic Handling Assistant (Festo, Esslingen am Neckar, Germany) while gripping and manipulating different objects.
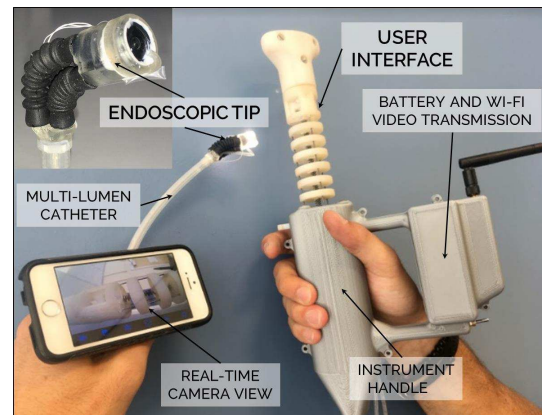
Fig. 1: The dual-continuum endoscope: Two continuum structures (i.e. a multi-backbone user interface and a pneumatically actuated endoscopic tip) are connected via syringes integrated in the instrument handle and a multi-lumen catheter.

In this paper, we propose to combine the benefits of multi-backbone continuum structures and soft robotic devices to design intuitive, low-cost, and portable endoscopes for visual investigation of the UGI tract. This work extends from the modeling adaptation presented in [35] of a PBA-based robotic endoscope, to design a stand-alone, purely mechanical dual-continuum endoscope (DCE) that possesses high intuitiveness of operation and low fabrication costs. Referring to Fig. 1, our design approach consists of a multi-backbone joystick (user interface – UI) coupled with an endoscopic tip (ET) oriented via a three-element PBA. Connection between the two units is obtained via passive pneumatic components only (i.e. syringes integrated in the instrument handle).

Beyond the innovation in design and the pre-clinal validation of the proposed approach, a contribution of the paper is proposing an analytical coupling of two continuum structures with different actuators (i.e. parallel bellows and multi-backbone in the presented case). The model-based approach builds upon a non-trivial preliminary calibration of a pneumatically actuated continuum tip. This method reduces the coupling problem of two dissimilar continuum structures to a single parameter. Additionally, it allows the ET response to be tuned to the operators input, facilitating direct user-to-task mapping for improved intuitiveness of operation.

II. Clinical and Technical requirements

The design of FE's have remained unchanged for over 60 years [36]. While they are used every day around the globe for the diagnosis and treatment of gastrointestinal disorders, FE's are not a perfect tool. In many cases, the design of traditional FEs limit their potential – especially in positively disrupting work-flow, improve patient access, and enhance patient care. When designing a novel FE specific for upper gastrointestinal tract exploration, many features need to be considered. These include:

1) WORKSPACE: Upper endoscopes (also known as gastro-scopes) are FEs specifically designed for use in the UGI tract. The tip of the upper endoscope can be deflected with 2 degrees-of-freedom (DOF) (210° max up and 90° max down with one knob; 100° max left and 100° max right with a second knob [37]) that yields a curvature radius of approximately 40 mm. Manipulation of the endoscopes insertion tube provides two additional degrees of freedom – endoscope advancement and withdrawal and rotation of the instrument along its main axis.

2) STIFFNESS: The stiffness of the FEs insertion tube ranges within 160-240 Ncm^2, measured as a product of Young modulus and second moment of area [38], depending on the exact upper endoscope selected. Unfortunately, this stiffness can lead to unintended adverse events including perforation of the tissue that has a high mortality rate (approximately 25%) [39].

3) DIAMETER: Standard upper endoscopes are 8-9 mm in diameter. Small- (7 mm) and ultra-small (3-4 mm) diameter upper endoscopes are commercially available – although are considered specialty endoscopes and are not present in all endoscopy units. The advantage of endoscopes smaller in diameter is that the upper GI tract can be examined with administration of a topical anesthetic to mitigate the gag-reflex and without conscious sedation or monitored anesthesia care [40], [41]. In addition, these can be inserted trans-nasally and advanced down to the hypopharynx, past the upper esophageal sphincter, into the esophagus, and then to the stomach and small intestine. In this manner, examination of the GI tract can be performed solely with use of a topical anesthetic. Therefore, the major advantage of a smaller diameter endoscope is to avoid the most common cause of adverse events in upper endoscopy, i.e. sedation [42].

4) ANATOMY: The esophagus, stomach, and first part of the small intestine (duodenum) comprise the upper GI tract. The esophagus is a hollow organ that is approximately 25 cm in length and 2 cm in diameter. The stomach is a J-shaped hollow organ that is approximately 10 cm in width and 30 cm in length along its longest axis [43]. The stomach has 6 key landmarks (i.e. gastro-esophageal junction (GEJ)/cardia, antrum greater and lesser curvature (AGC and ALC), body greater and lesser curvature (BGC and BLC), and fundus) that are typically inspected during an EGD. The duodenum is a c-shaped structure between the bulb and second portion followed by a straight segment for the third and fourth portions. The duodenum is approximately 2.5 cm in diameter and 30 cm in length. The surfaces of these segments are moist and can have fluid, mucous, and debris. The hollow structures are also collapsed at rest unless air or other gas is introduced. Therefore, the upper endoscope must possess the ability to irrigate, aspirate, rinse the camera lens, and insufflate the lumen to allow for space creation and adequate mucosal visualization.

5) USABILITY: Medical providers undergo extensive training in order to be able to perform endoscopy in a competent manner. Due to the design of the endoscope, there is a steep learning curve and a real potential for adverse events if one is not well trained [39]. This learning curve and non-intuitive dual-knob controlled actuation mechanism limit the number of providers who are able to competently perform the procedure [44], [45]. Hence, there exists a true shortage of providers whom are able to perform endoscopy for an ever-expanding population of patients who need the procedure. In addition, endoscopists must be well-trained in order to be able to compensate for the 13-25° tip bending error associated with traditional FEs [37] and avoid adverse events.

6) PORTABILITY: The traditional FE tower is comprised of a box light source, image processor, monitor, computer, computer monitor, irrigation pump, and, in most current set-ups, a CO_2 insufflation system that are arranged on a large cart with wheels (range: 60-120 cm width, 115-125 cm tall, 60-65 cm deep). This system is bulky, heavy, and burdensome to transport. In addition, the system must be connected to a wall-power supply and suction mechanism. The physical size and encumbrance of the traditional FE platform alone limits its use to larger rooms/suites in the medical setting and prohibits it in patient care rooms or outpatient clinics.

A stand-alone endoscopic device that is lightweight, portable, small in physical size, does not rely on a fixed power supply, and can be viewed on a personal device (i.e. smart phone, tablet, etc.) has the potential to provide a solution for screening in outpatient clinics, at the bedside in patient care units in medical centers, and in rural/remote locales around the globe.

7) COST: In the US, the average total cost of an upper endoscopy is 1,775 USD per procedure [1] with an average endoscope reprocessing cost of 160 USD per case [6]. The approximate upfront capital cost for an upper endoscopy tower is 80,000 USD, while for an automated endoscope reprocessing system is 40,000 USD. Therefore, these capital and recurrent costs make traditional upper endoscopy cost prohibitive outside of dedicated endoscopy units and for many low- and middle-income countries around the world.

8) DURATION OF THE PROCEDURE: An average diagnostic EGD can be completed in 4 to 12 minutes. The total time spent by a patient in an endoscopy facility can be between 60-120 minutes, as this includes the pre-procedure/sedation assessment, sedation recovery, and discharge.

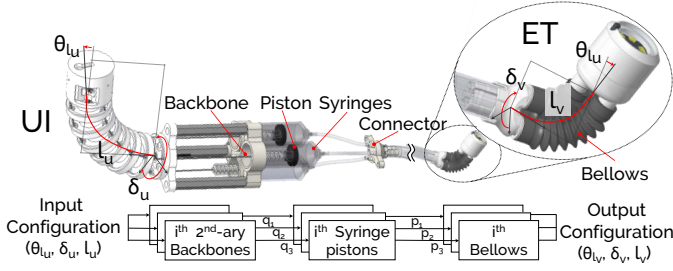## III. PRINCIPLE OF OPERATION: DUAL-CONTINUUM ENDOSCOPE

Fig. 2: Functional components of the dual-continuum endoscope implementing a direct user-to-task mapping: the user interface (UI) is mechanically coupled to the endoscopic tip (ET).

Referring to Fig. 2, the DCE is composed of a mechanically actuated UI and a pneumatically actuated ET that are coupled through a mechanical-pneumatic interface.

The UI is a snake-like multi-backbone continuum joystick adapted from [18], [19] to allow for extensibility in a longitudinal DOF in addition to the two DOF of bending in any direction. Superelastic Nitinol rods are used as primary and secondary backbones of the UI. The primary backbone is centrally located and surrounded by three radially equidistant secondary backbones whose extension/retraction corresponds with the three DOF of the UI. As the user manipulates the UI, changing its configuration (i.e. bending angle θ_{l_u}, the angle of the plane in which the UI bends δ_u, and the nominal length l_u), the superelastic backbones extend or retract at their distal ends, which are connected directly to three syringe pistons. The motion of each syringe piston results in pressurization/depressurization of one of the three pneumatic lines coupled via a multi-lumen catheter to a corresponding bellow in the PBA. Pressure changes extend/retract the PBA bellows, resulting in a specific output configuration of the ET (i.e. θ_{l_v}, δ_v, and l_v).

Coupling kinematically-similar structures in the UI and ET has the advantage of providing a direct user-to-task mapping through pure mechanical actuation, allowing for highly intuitive operation upon proper tip response tuning.

IV. KINEMATIC MODELING TOWARD DIRECT USER-TO-TASK MAPPING

Extensible multi-backbone continuum robots had been proposed in [46], while a detailed analysis of their inherent capabilities was done in [47]. Using appropriate kinematic description, it is possible to determine a relationship between UI and ET, and use this to tailor design variables to achieve a desired mapping between input and output configurations.

The kinematic modeling of a continuum segment aims to describe the relationship between *joint space*, described by the actuator input parameters (UI backbones or ET bellows extension/retraction), $\mathbf{q}$, and the *task space* identified by the end effector pose, described by $[\mathbf{p}, \mathbf{R}]$ where $\mathbf{p} = [p_x, p_y, p_z]^\mathrm{T}$ represents the Cartesian position of the end effector, and $\mathbf{R} = {}^b\mathbf{R}_e$, $\mathbf{R} \in \mathrm{SO}(3)$ represents the rotation matrix between end effector frame $\{e\}$ and base frame $\{b\}$ of the segment.
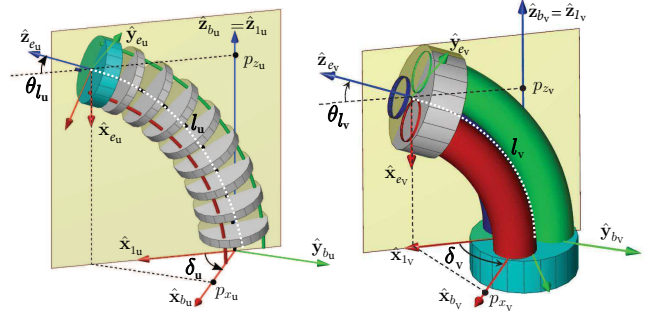

Fig. 3: Kinematic nomenclature of continuum structures. Left: schematic model of the UI; Right: schematic model of the ET.

To achieve such relationship, a third space is used: the *configuration space* [20]. The configurations space variables, $\boldsymbol{\psi} \triangleq [\theta_l, \delta, l]^\mathrm{T}$, refer to the geometric values that characterize the shape of the continuum segment. Task and configuration space variables are shown in Fig. 3 for both the UI and ET schematic models. The subscripts $_u$ and $_v$ refer to variables associated with the UI and ET, respectively.

Hence, to describe the tip pose as a function of the joint variables (and vice versa), two kinematic mappings have to be defined: the mapping from configuration space to task space, and the mapping from configuration space to joint space. These are presented in equations (1) and (2), respectively.

$$\mathscr{F}_\mathrm{T}: \quad \boldsymbol{\psi} \rightarrowtail [\mathbf{p}, \mathbf{R}] \qquad \text{config. to task space} \quad (1)$$

$$\mathscr{F}_\mathrm{q}: \quad \boldsymbol{\psi} \rightarrowtail \mathbf{q} \qquad \text{config. to joint space} \quad (2)$$

A. UI - Multi-backbone Mappings

The mappings of multi-backbone continuum robots in the form of the UI are:

1) $\mathscr{F}_T$ - configuration to task space: The position vector $\mathbf{p_u}$ and the rotation matrix $\mathbf{R_u}$ are related to the configuration parameters using equations (3) and (4), respectively [18]. The terms $c_{(\cdot)}$ and $s_{(\cdot)}$ denote the cosine and sine functions; $[\mathbf{z_{e_u}}^\wedge]$ represents a skew symmetric matrix generated from $\mathbf{z_{e_u}}$-axis of the end effector pose; the variable s denotes the curve length along the primary backbone (main axis); and θ_0 is the initial bending angle ($\theta_0 = \frac{\pi}{2}$; i.e. straight configuration). The parameters L_- and L_+ denote the minimum and maximum lengths of the primary backbone respectively.

$$\mathbf{p_u} = e^{-\delta_u[\mathbf{z_{e_u}}^\wedge]} \int_0^{l_u} [c_{(\theta_s)}, 0, s_{(\theta_s)}]^\mathrm{T} \, \mathrm{d}s, \quad l_u \in [L_-, L_+] \quad (3)$$

$$\mathbf{R_u} = e^{-\delta_u[\mathbf{z_{e_u}}^\wedge]} e^{(\theta_0 - \theta_{l_u})[\mathbf{y_{e_u}}^\wedge]} e^{\delta_u[\mathbf{z_{e_u}}^\wedge]} \quad (4)$$

The bending angle along the curve length (θ_s) can be determined using equation (5), where $\kappa(\nu)$ describes a generic curvature function. Assuming constant curvature, $\kappa(\nu)$ is invariant (as in equation (6)). Therefore, the bending angle $\theta(s)$ can be described as in equation (7):

$$\theta(s) = \theta_0 + \int_0^s \kappa(\nu)\mathrm{d}\nu, \quad s \in [0, l_u] \quad (5)$$

$$\kappa(\nu) = (\theta_{l_u} - \theta_0)/l_u \quad (6)$$

$$\theta(s) = \theta_0 + (\theta_{l_u} - \theta_0)s/l_u = \theta(s, l) \quad (7)$$

This formulation provides a complete description of the pose of the end effector using only the configuration parameters and initial bending angle θ_0.

2) $\mathscr{F}_q$ - configuration to joint space: The configuration to joint space mapping relates instead the joint variable $\mathbf{q_u}$, given the configuration variable $\boldsymbol{\psi_u}$ [18]. The joint variables represent the change in length (elongation/contraction) of the secondary backbones and are defined as follows:

$$q_{u_i} = l_i - l_{u_0}, \qquad l_i = l_u + \Delta_i(\theta_{l_u} - \theta_0) \tag{8}$$
$$\Delta_i = r_u \cos \sigma_i, \qquad \sigma_i = \delta_u + \tfrac{2\pi}{3}(i-1), \quad i \in [1,3] \tag{9}$$

The parameter l_{u_0} represents the initial joint length, the variable l_u represents the main axis (primary backbone) length, and the calculated expression l_i represents the length of the ith joint. The term r_u is the distance in the base plane between secondary backbone axes and primary backbone axis.

B. ET - PBA Actuation Compensation Mapping

In [35], the same ET was modeled taking inspiration from [30], [34] for their work on PBAs and from [48], [49] for their contribution to transmission loss compensation. As detailed in [35], we adapted the modeling method from existing multi-backbone continuum robots such that the two mappings defined for describing the UI, also hold for the ET with differences only in fabrication parameters (e.g. r_v identifies distance between bellows center line and manipulator virtual main axis, and l_v is the length of the imaginary center line of the three bellows; l_{v_0} represents the length of the bellows at neutral pressure).

From a fabrication standpoint, the joint variable $\mathbf{q_u}$ represents the mating component of the two structures, i.e. the piston displacement. This displacement, which is responsible for bellows' extension $\mathbf{q_v}$, may suffer from transmission losses due to the compressibility of air, used as transmission medium, and the compliance of the bellows.

A schematic representation of the actuation losses and compensation methods is shown in Fig. 4. To model the
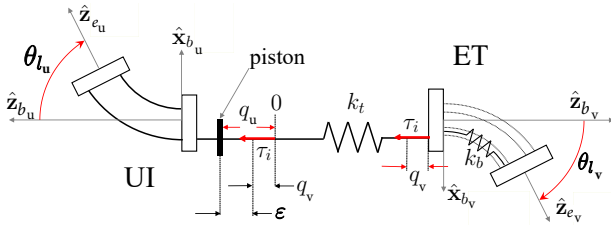

Fig. 4: Schematic representation of motion transmission modeling associated with a piston extension ε.

configuration mapping, a piston extension term ε is introduced such that:

$$\mathbf{q_u} = \boldsymbol{\varepsilon} + \mathbf{q_v} \quad \boldsymbol{\varepsilon}, \in \mathrm{I\!R}^3 \tag{10}$$

In the following, we assume: 1) a linear relationship between bellows length variation $\mathbf{q_v}$ and line pressure, and 2) a negligible friction through the transmission line.

Using the first assumption, we can relate the actuation forces $\boldsymbol{\tau}$ at the base of each bellow to a nominal longitudinal stiffness k_{b_i} as:

$$\boldsymbol{\tau} \triangleq [\tau_1, \tau_2, \tau_3]^{\mathrm{T}}, \quad \tau_i = p_i A = k_{b_i}(l_i - l_0), \quad i \in [1,3] \tag{11}$$

Considering the fluid compression as a spring having a stiffness of k_t and using the second assumption of frictionless transmission, we have $\tau_i = k_t \varepsilon_i$. Equating it and (11), yields:

$$\boldsymbol{\varepsilon} = [\varepsilon_1, \varepsilon_2, \varepsilon_3]^{\mathrm{T}}, \quad \varepsilon_i = k_{\varepsilon_i} q_{v_i}, \quad k_{\varepsilon_i} \triangleq (k_{b_i}/k_{t_i}) \tag{12}$$

where a dimensionless gain k_{ε_i} is introduced for simplicity, and defined as the ratio between the stiffnesses of each bellow and the corresponding transmission line. Therefore equation (10) can be rewritten as:

$$\mathbf{q_u} = (1 + \mathbf{K}_\varepsilon)\mathbf{q_v} \tag{13}$$

where $\mathbf{K}_\varepsilon$ is a 3x3 diagonal motion compensation matrix accounting for motion losses in each pneumatic line:

$$\mathbf{K}_\varepsilon, \in \mathrm{I\!R}^{3\times 3}, \ \mathbf{K}_\varepsilon = \mathrm{diag}\left(\mathbf{k}_\varepsilon\right), \ \mathbf{k}_\varepsilon \in \mathrm{I\!R}^3 \tag{14}$$

The addition of a motion compensation matrix allows the description of the ET configuration as a function of the piston displacement $\mathbf{q_u}$.

C. UI-ET Compensated Coupling

To achieve a target mapping of 1:1 between the UI-ET coupling that includes compensation for motion loss, equation (13) can be reformulated to contain the tunable design parameters r_u and r_v. This involves combining equations (8) and (9), considered for both the UI and ET, with equation (13) under the assumption that: 1) following ET deployment in the stomach, the third DOF in elongation is not available nor necessary (i.e. $l_u = l_{u_0}$ and $l_v = l_{v_0}$); 2) the bending angles and bending directions for UI and ET are equal (i.e. $\theta_{l_u} = \theta_{l_v}$ and $\delta_u = \delta_v$). Hence, the design variables may be related as:

$$\mathbf{r_u} = (1 + \mathbf{K}_\varepsilon)\mathbf{r_v} \tag{15}$$

The gain $\mathbf{K}_\varepsilon$ may be experimentally determined for a given set of DCE components/design parameters. To minimize the dimension of the ET and couple the UI accordingly, we must maintain a constant kinematic radius (i.e. $\mathbf{r_u} = r_u\,[1\,1\,1]^{\mathrm{T}}$ and $\mathbf{r_v} = r_v\,[1\,1\,1]^{\mathrm{T}}$). Thus, the compensation matrix may be simplified to a single scalar gain $\bar{k}_\varepsilon$ determined by averaging elements $(\mathrm{diag}\,(\mathbf{k}_{\varepsilon_i}))$, therefore obtaining:

$$r_u = (1 + \bar{k}_\varepsilon)r_v \tag{16}$$

Equation (16) is fundamental for achieving a 1:1 mapping between UI and ET, while compensating for motion losses and taking into consideration the physical constraints of the target device (e.g. syringe spacing, ET maximum dimension and UI ergonomics).

V. Design Considerations and Fabrication

A. Experimental Determination of $\mathbf{K}_\varepsilon$

Our eventual design goal is to obtain a UI that comfortably fits within the user's hand while offering a direct user-to-task mapping between the UI and ET. With the bellows size fixed for the ET due to space considerations ($r_v = 4\ mm$ as described in Section V-B1), the open design parameters included the kinematic radius r_u of the UI and the syringe sizes. Small syringes would require a larger stroke and have smaller compressible volume, while large syringes require a smaller stroke, but use more compressible volume and therefore exhibit larger motion transmission losses. However, the motion compensation gains for each syringe depend on the compressible volume and the displaced volume - therefore it is not immediately clear what syringe size should be chosen *a-priori*. With the stroke size directly related to r_u, it was important to experimentally explore different syringe sizes to discern which would correspond with a feasible design.

A controllable experimental platform, shown in Fig. 5(a), was developed to evaluate the expected transmission motion compensation matrices $\mathbf{K}_{\varepsilon_i}, i = 1, 2, 3$ corresponding with syringe volumes 3 ml, 5 ml and 10 ml. The average motion compensation gain $\bar{k}_\varepsilon$ was determined and used to set the desired secondary backbone radius r_u in accordance with equation (16). The most appropriate syringe size was subsequently selected based on an r_u that allowed for parallel alignment of the syringes and delivered a UI size that could comfortably fit within the users hand.

To control the platform, a host machine communicates via Ethernet to a Matlab Simulink™ real-time xPC target environment. The target machine is programmed to communicate with an electromagnetic (EM) tracking system (Mid Range Transmitter, 3D Guidance trakSTAR - Ascension, NDI, Waterloo, Canada) at 125 Hz, and with a Data Acquisition (DAQ) board (SCB-68, National Instrument, Austin, TX, USA) at 5 kHz.

To determine the compensation matrix $\mathbf{K}_\varepsilon$, the change in ET pose as a function of known piston position was recorded. Position and orientation of the ET $[\mathbf{p_v}, \mathbf{R_v}]$ was monitored using 6-DOF EM trackers. The ET was assembled with a temporary 3D printed part to allow reliable attachment of the EM sensors. It is worth mentioning that the 3D printed parts have comparable weight (1.25 g) to the device camera used later for validation.

To achieve accurate and repeatable control of the syringe piston positions, stepper motors (Nema17 17HS16-2004S, OMC Corporation, Nanjing City, China) were used to actuate a mechanical drive-train. The 200 steps per revolution stepper motors were connected to lead screw of $1.59mm$ pitch, and driven via an 8 micro step per step driver (Big Easy Driver, Sparkfun Electronics, Boulder, CO, USA). When triggered through the DAQ board, the drive system achieved a linear resolution at the piston of $0.99\mu m/\text{step}$. Potentiometers were used to define initial testing (home) positions, to improve repeatability of the experiments.

For each of the syringe sizes, $\mathbf{K}_\varepsilon$ was determined through combining ET pose and piston position data into an iterative linear least-squares problem. Bending angle data were con-

tinuously acquired ($\Theta_{des} \in [10°, 70°]$) on 5 equally spaced bending planes ($\delta_{des} \in [0°, 120°]$ - due to symmetry in the workspace). Starting from an uncompensated scenario (i.e. $\mathbf{k}_\varepsilon = [0\,0\,0]^T$), the compensation terms were calculated off-line using an iterative least squares method as proposed in [35]. The compensation terms were then updated in the model to acquire a new set of data until a threshold of 2% increment between the new and previous compensation terms was satisfied (relative convergence criterion).
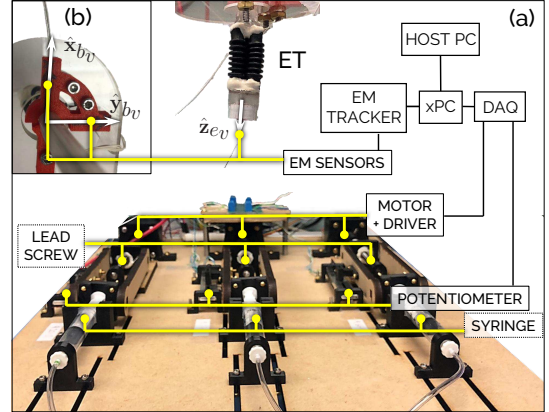

Fig. 5: Experimental setup: (a) An xPC machine controlling the actuation system (stepper motor - potentiometer - lead screw - syringes) via Data Acquisition Board (DAQ), and tracking tip position ($\hat{\mathbf{z}}_{e_v}$) using EM sensor\tracker; (b) Base frame $\{b\}$ was defined before the experiment routine by acquiring the $\hat{\mathbf{x}}_{b_v}$ and $\hat{\mathbf{y}}_{b_v}$ axis and used as reference for tip position estimation.

In Fig. 6, the measured bending angle (Θ_{meas}) as a function of desired bending angle (Θ_{des}) is shown for the three syringe sizes investigated.

As visible from the plots, all bending motions present hysteresis and a non-linear behavior once Θ_{meas} exceeds $65°$ (for the compensated scenario). The former is a common effect of pneumatic actuation, and is thought not to compromise the use of the device; the latter instead is a consequence of the radial expansion (ballooning) of the bellows, i.e. violation of linear relationship between pressure and elongation. Also evident in Figure 6 are small ripples in the acquired data. These deviations were found to be random in nature for piston location and between repeats. Therefore, are assumed to be caused by friction dynamics occurring at the piston-syringe wall interface under slow linear motion, and backlash of the mechanical drive train.

Table I shows the vectors of motion compensation $\mathbf{k}_\varepsilon$ as first mentioned in equation (14) along with the scalar gains $\bar{k}_\varepsilon$, which were defined as the mean of $\mathbf{k}_\varepsilon$ for each syringe size. The corresponding UI kinematic radii r_u predicted for direct mechanical-pneumatic mapping, determined without compensation (i.e. $r_u = r_v$) and with compensation (equation (16)), are also reported. For each syringe size assessed using motion loss compensation under robotic control, implemented according to Eq. (13), a large reduction in bending angle Root Mean Squared Errors (RMSE_{θ_l}) was evident. For example, the RMSE_{θ_l} were less than $7°$ for each tested syringe size after motion loss actuation compensation was implemented.
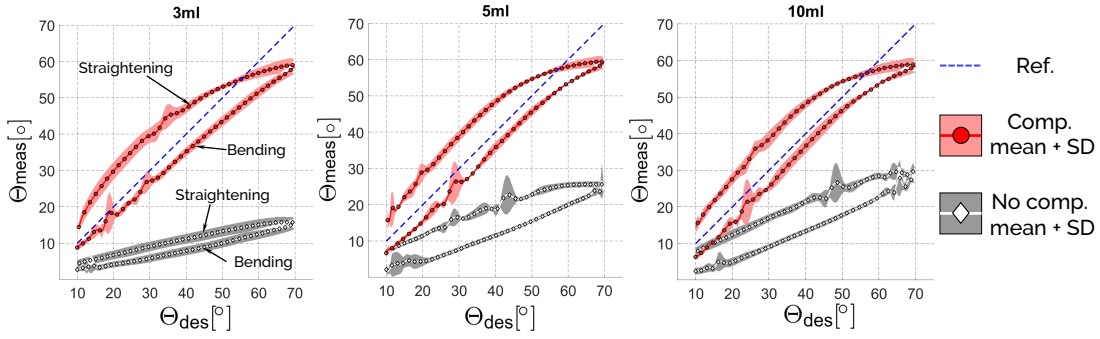
Fig. 6: Measured bending angle (Θ_{meas}) as a function of desired bending angle (Θ_{des}) before (diamonds-grey) and after (circles-red) compensation for the three syringes sizes investigated.

TABLE I: Motion loss compensation gains and required UI kinematic radius for direct coupling for three syringe sizes.

Syringe size	3 [ml]	5 [ml]	10 [ml]
Syringe diameter	8.6 [mm]	12.0 [mm]	14.6 [mm]
$\mathbf{k}_\varepsilon$	$\begin{bmatrix} 2.97 \\ 3.19 \\ 3.62 \end{bmatrix}$	$\begin{bmatrix} 1.46 \\ 1.55 \\ 1.59 \end{bmatrix}$	$\begin{bmatrix} 1.35 \\ 1.42 \\ 1.34 \end{bmatrix}$
$\bar{k}_\varepsilon$	3.26	1.53	1.37
Not Compensated coupling: $r_u = r_v, q_u = q_v$, i.e. $\mathbf{K}_\varepsilon = \mathbf{0}$			
r_u[mm]	4.04	4.04	4.04
RMSE$_{\theta_l}$[°]	33.36	27.13	25.18
Compensated coupling: $r_u > r_v$, i.e. $\mathbf{K}_\varepsilon = diag(\bar{k}_\varepsilon)$			
r_u [mm]	17.21	10.25	9.57
RMSE$_{\theta_l}$ [°]	6.97	6.40	6.30

These results were used to inform the final choice of design parameters for the fabricated UI. In particular, we designed a UI using 5ml syringes and a kinematic radius $r_u = 10.25mm$ to obtain a suitable UI continuum segment dimension and feasible parallel arrangement of the syringes within a small UI body. The UI was hence fabricated and assembled with the selected syringe size to validate the direct user-to-task mapping when direct mechanical-pneumatic coupling is used.

B. Fabrication and Integration of the UI with the ET

The UI syringes were connected to the PBA of the ET using a multi-lumen silicone catheter. The device was designed to facilitate detachable coupling between the two, and was therefore split into disposable and reusable assemblies.

The ET, along with the multi-lumen catheter, comes in direct contact with the patient's bodily fluid, while the syringes used for actuation may come into contact indirectly, e.g. in the case of perforation/tear in the catheter/bellows. Hence these items must be disposed of to prevent costs associated with device reprocessing.

The entire UI can instead be reused due to a modular coupling between the backbone free ends and the syringe pistons. As represented in Fig. 1, the UI is embedded in a 3D printed case that contains reusable electronics. Specifically, a rechargeable battery (Ni-MH 2A 12V 1800MAH) and Wi-Fi transmission module (WishRing Wifi, Amazon.com). The former is used to remove the need for an external power supply, and the latter to provide users with a real-time camera view on a smartphone or a tablet.

1) Disposable parts (ET and Catheter): As shown in Fig. 7(a), the ET is comprised of a plastic adapter (connecting the catheter to the bellows), three rubber bellows, and a plastic camera housing. All plastic parts were 3D printed (Clear resin V2, FormLabs Somerville, MA, USA) and attached to the catheter and bellows using an epoxy glue (Loctite Marine Epoxy). Three off-the-shelf bellows (BC-2305, Rubberstore, Vandalia, OH, USA) were aligned to minimize the overall diameter (this resulted in $r_v = 4$ mm) (Fig. 7(b)).

The camera housing contains a 1.3 Megapixel camera (RA78080A-60 Bangu Technology Development CO., Baoan, China) and three light emitting diodes (LED) for illumination (EAHC2835WD4, Everlight Electronics, Taipei, Taiwan). The assembled ET has an outside diameter of 13.5 mm.

The flexible catheter was fabricated through silicone extrusion (Nusil MED4880-silicone) to a diameter and length of 7 mm and 120 cm, respectively. A cross-sectional view of the catheter, shown in Fig. 7(a), illustrates the geometry of the 7 internal channels. Six circumferential channels are used for: camera and lighting wires (x1); insufflation (x1); irrigation and lens cleaning (x1); and pressure lines for the three rubber bellows of the tip (x3). The flexural strength of the catheter was eastimated to be $< 34.83\ Ncm^2$ (given a material Young modulus of 7.1 MPa, and assuming a solid rod of 5 mm in diameter), which is 6 times less than a traditional FE.

Highly flexible tubing (6 Fr, 0.003 wall thickness Pebax-35D, Apollo Medical Extrusion, Sandy, UT, USA) and wires (Calmont, Santa Ana, CA, USA) are used for irrigation and for electrical connection with the camera module, respectively. These components bypass the PBA without compromising the range of motion of the ET.

At the proximal end of the catheter, a second plastic adapter provides access to each catheter's lumen. The three bellows pressure lines are directly connected via PVC tubing to three syringes. The syringe centers (Fig. 7(d)) are aligned with a 120° angular offset to the secondary backbone circumference (i.e. r_u). Access to the irrigation and insufflation channels at the proximal end is provided via tubing and standard luer-lock adapters for connection to external water and air supply.

2) Reusable parts (UI and Case): The UI components, shown in Fig. 8, are:

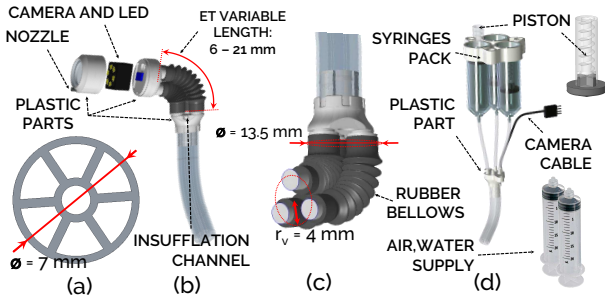A. 3D printed spacer discs (six in total).

Fig. 7: Disposable Parts: (a) Cross section of the multi-lumen catheter; (b) ET exploded view; (c) PBA; (d) Proximal end of the scope, syringe pack.
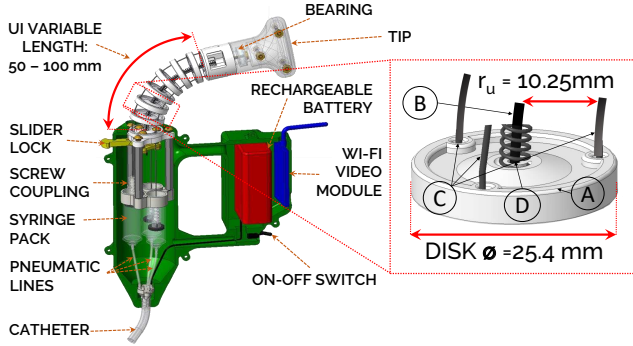

Fig. 8: The reusable user interface (UI) showing key components, and the backbones with spacer disk (inset).

B. A $\varnothing 1.5$ mm Nitinol wire as primary backbone located in the disc center.

C. Three $\varnothing 1$ mm Nitinol secondary backbone wires equispaced ($120°$ offset) around the circumference of a circle of radius r_u.

D. A 3.33 lbs/in compression spring (compressed length = 48% of initial length) used as inter-discs spacer ($7mm$).

The kinematic model we used assumes no twisting of the UI. To minimize this in the physical device, we used a ball bearing (B623B1E, IGUS, Cologne, Germany) to connect the UI tip to the multi-backbone continuum structure, as shown in Fig. 8. Alternative mechanical solutions such as adding additional secondary backbones not used for actuation can be implemented to improve structural resistance to torques acting on the main axis.

A custom 3D printed screw coupling provides adjustable connection between the UI and the syringe pistons. Each screw, glued to the corresponding secondary backbone distal end, fits a nut on a custom piston, providing ease of separation between disposable and reusable parts.

A stiffer ET is useful during introduction via the esophagus and when navigating through shrinkages and complex anatomies. To lock the ET into a stiffer configuration (i.e. PBA completely depressurised), a slider lock mechanism (see Fig. 8) was integrated into the base of the UI. As the user pulls the UI to depressurise the PBA and a certain extension is reached, the slider lock mechanism can be engaged, locking the primary backbone.

3) Fabrication cost: Table II summarizes both fabrication cost for a single functional prototype and the unit cost considering mass production (MP). MP costs were estimated by

TABLE II: Prototyping and estimated mass production cost of the DCE.

Part	Prot. Cost [USD]	Est. MP Cost [USD]
Disposable components		
Plastic parts	0.54	**0.25**
Multi-lumen catheter	3.71	**0.30**
Wiring and connector	2.15	**1.00**
Bellows	13.74	**3.00**
Tubing	0.33	**0.20**
Syringes and pistons	1.78	**1.00**
Camera and LEDs	17.02	**4.00**
Total cost for disposable parts	39.27	**9.75**
Reusable components		
Plastic parts	41.43	**5.00**
Screw-bolts, standoffs	9.54	**5.00**
Nitinol wires and spring	24.95	**3.00**
Bearing	2.31	**1.00**
Rechargeable batteries	32.22	**5.00**
Wi-Fi video transm.	39.96	**10.00**
Total cost for reusable parts	150.41	**29.00**

discussing the DCE design with a medical device manufacturer (Medical Murray, North Barrington, IL, USA). The two categories are subdivided into disposable and reusable parts. From Table II, it is evident that even at the prototyping stage, the cost associated with the disposable parts of the device are 76% less than of the reprocessing cost identified in [6]. With increased economy through mass production, the cost can be further reduced down to <30 USD for the reusable equipment and <10 USD for disposables.

For both the prototype and MP scenarios, the camera represents the most significant cost. Although it is economically feasible to consider this as disposable, the design may be adjusted to accommodate a reusable camera, as implemented in [13], [50], thus further cutting disposable costs to <6 USD.

VI. EXPERIMENTAL VALIDATION

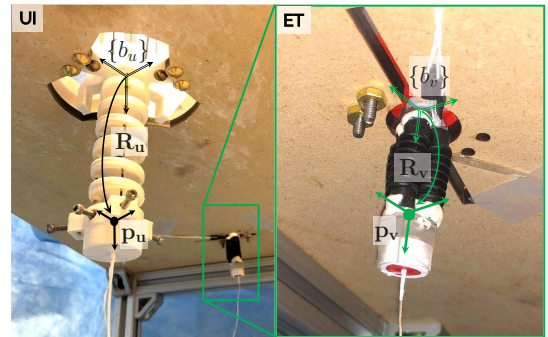### A. Experimental assessment of user-to-task mapping

Fig. 9: Experimental set up for validation of user-to-task mapping. UI and ET were tracked while the UI was manipulated by hand within the input workspace. A zoomed view of the ET is reported on the right.

To verify that we achieved the intended direct mapping through the selected design parameters, we placed the UI and ET next to each other on a dedicated bench test setup shown Fig. 9. Both end effectors of the UI and ET were magnetically tracked when the UI was moved by hand. The end effector positions and orientations ($[\mathbf{p_u}, \mathbf{R_u}]$, and $[\mathbf{p_v}, \mathbf{R_v}]$ respectively) were obtained relative to their own respective base frames $\{b_u\}$ and $\{b_v\}$. Similarly to the experimental set up used in V-A, a 3D printed part having comparable

weight (1.25 g) to the device camera was used for EM sensor placement at the ET end effector. The UI and ET were initially aligned in a parallel configuration ($\{b_u\} = \{b_v\}$). Starting from an initial alignment pose, the user manually bent the UI across a range of bending angles Θ_u ($\Theta_u \in [0°, 80°]$) in different planes δ_u ($\delta_u \in [0°, 360°]$).

The imposed bending angles (Θ_u) and bending planes (δ_u) of the UI and the corresponding response of the ET (Θ_v and δ_v) are shown in Fig. 10, with the bending angles (Θ) and bending planes (δ) being shown in Fig. 10(a) and (b), respectively. The RMSE $\pm$ Standard Deviation (SD) for bending angle Θ tracking was $5.35° \pm 3.17°$ within the linear regime ($\Theta_u \in [0°, 65°]$), while the RMSE $\pm$ SD on δ tracking was $15.87° \pm 15.57°$ (values calculated once an imposed bending angle ($\theta_{l_u} > 15°$) was established, due to numerical imprecision in calculating both δ_u and δ_v when the manipulators are straight).

These errors may be attributed to a number of factors including the mechanical tolerances within the assembled device, the hysteresis within the ET pressure-bending profile, and the necessity to average the compensation parameters into a single value for the UI design.
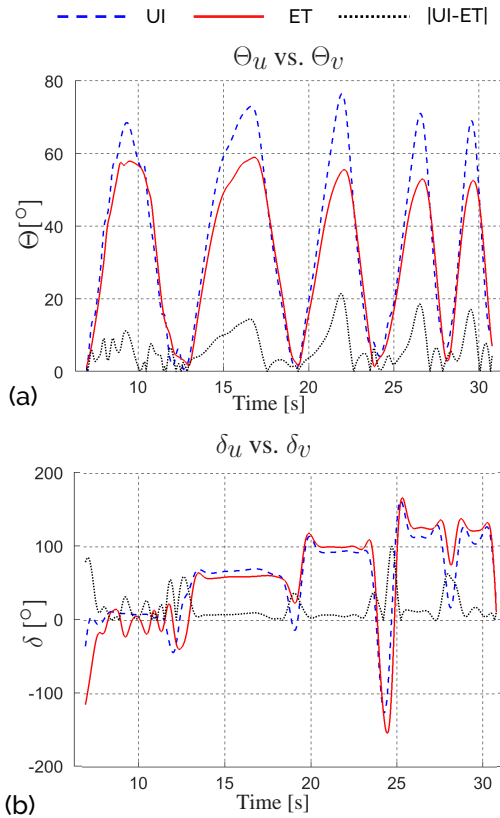

Fig. 10: Results from experimental validation of direct user-to-task mapping. Continuous (red) lines are related to the ET, dashed (blue) lines are related to the UI, dotted (black) lines represent the instantaneous error between the ET and UI motions. (a): Θ_v tracking Θ_u; (b) δ_v tracking δ_u.

B. Usability trial

To validate the clinical efficacy of DCE, visualization tasks of relevant landmarks (Section II-4) were performed in an anatomical simulator of the UGI tract using a conventional flexible endoscope as a benchmark.

One expert gastroenterologist (>3,000 lifetime EGDs) and ten non-expert users with minimal or no previous experience with FE were asked to perform landmarks visualizations in an instrumented UGI tract phantom using either the DCE or a conventional FE (Karl Storz - Tuttlingen, Germany) in a random order, and relying on direct camera feedback only. An UGI tract phantom, consisting of esophagus and stomach (dimensions taken from tomographic scans), was silicone molded (EcoFlex 00-30, SmoothOn, Macungie PA, USA) with six different color LEDs embedded at key landmark positions in the stomach (Fig. 11(a)). The time required to visualize each landmark was recorded for each run via a dedicated custom software application (Phython, Python Software Foundation, DE, USA) that communicated with a 6-button console and an embedded controller (Arduino Mega 2560, Arduino, Somerville, MA, USA). When a landmark was visualized, the corresponding button was pressed by the study observer to turn off the specific LED and the time recorded.

Both expert and non-expert users performed the trial 5 times with each device. Timing (median (Q2) [1st quartile (Q1) 3rd quartile (Q3)]) to visualize each and all landmarks are shown in Fig. 11(b) for the expert user, and in Fig. 11(c) for ten non-expert users, respectively.

The expert user took less time to complete landmark visualisation with the conventional FE compared to DCE (median 12.97s vs. 25.65s, respectively). The non-expert users were instead faster with the DCE when compared to conventional FE (36.97s vs. 46.11s, respectively), showing a comparable DCE performance to the expert user (36.97s vs 25.65s). The fact that non-expert users performed better with the DCE provides preliminary evidence of the improved usability of the proposed approach.

In addition, at the end of the trials, the non-expert users were asked which device they prefer for the visualization task, and for feedback on the DCE. All users found the DCE more intuitive, and simpler to control. The difference noted for the DCE, with respect to the conventional FE, were the smaller range of motion at the tip, the inability to couple insertion with steering (two hands actuation), and the lower stiffness of the insertion tube.

C. Pre-clinical assessment

A feasibility *in-vivo* trial comparing the DCE with flexible endoscopy was performed by an expert gastroenterologist (>3,000 lifetime EGDs) in a 40-kg Yorkshire female pig at Vanderbilt University, with the assistance and collaboration of a specially trained medical team, in accordance with all ethical considerations and regulation related to animal experiments (IACUC Approval No. $M1700034 - 00$). The results were discussed in [51] and are briefly summarised here. The user was able to perform a diagnostic EGD, and visualize the main landmarks in 180s using conventional FE and 208s with the DCE. There were no adverse events, evidence of endoscopic or gross trauma, perforation, or histologic abnormality at necropsy. To further evaluate the efficacy and usability of the
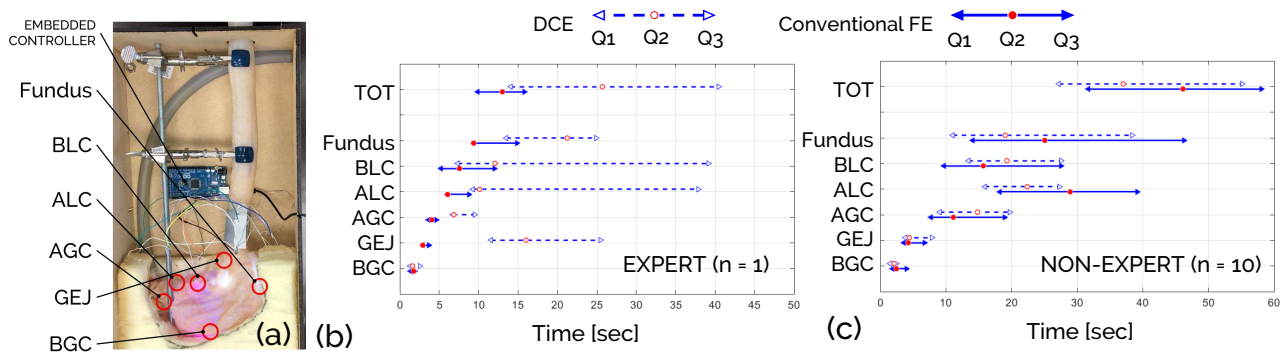
Fig. 11: Usability Trial: (a) UGI tract simulator used, where the red circles indicate the position of each LED/landmark; (b) Timing for expert using both conventional FE and DCE; (c) Timing for non-expert users using both conventional FE and DCE. In both (b) and (c) the y-axis of the plots reports the landmarks in the order shown in (a), and the red circle indicate the median times (Q2), while the left pointing triangle the first quartile (Q1) and the right pointing triangle the third quartile (Q3).
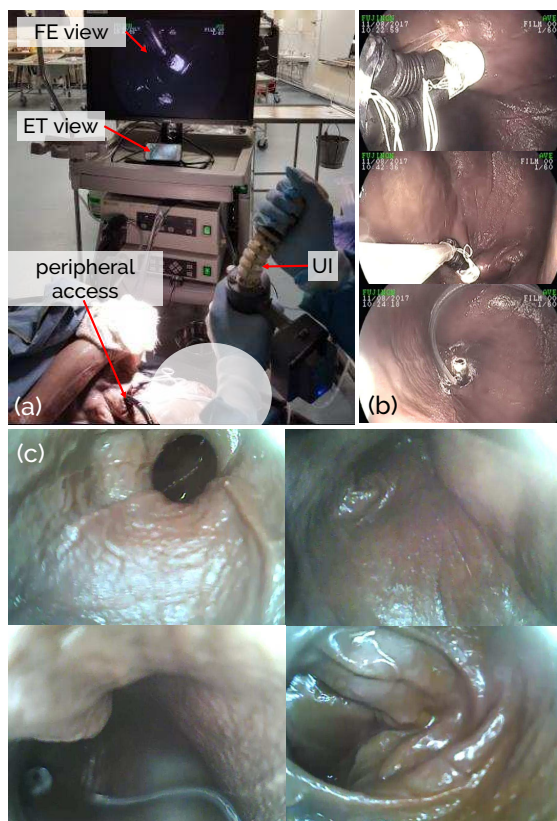

Fig. 12: Pre-clinical assessment of the DCE in a cadaver trial. (a) Experimental set up; (b) Motion of the DCE observed from the conventional FE; (c) Camera view from the DCE showing clockwise: gastro-esophageal junction, AGC and ALC, duodenum, and view during retroflexion.

DCE in visualizing the human anatomy, an EGD procedure was performed in a soft-tissue cadaver. The procedure was executed by an expert gastroenterologist (>3,000 lifetime EGDs) in a female Thiel-embalmed cadaver (48 kg) in the facilities of the School of Medicine at the University of Leeds, with the assistance and collaboration of a specially trained medical team and in accordance with all ethical considerations and regulation related to cadaver experiments (Approval No. $AEC - 2017 - 080617$).

First, the anatomy was explored using a conventional FE

(GIF-H290, Olympus Corp., Tokyo, Japan), and then the DCE was introduced. The cadaver presented a very small anatomy of the pharynx that prevented navigation through the throat for both devices. To obviate this problem, the throat was bypassed with a peripheral access incision performed in the neck to feed both devices in the proximal section of the esophagus (Fig. 12(a)). The ET camera view was transmitted directly via WiFi to a smartphone (iPhone, Apple, USA) and a tablet (iPad, Apple, USA) located on the endoscopic tower.

The DCE successfully reached the stomach in a stiffened configuration (i.e. bellows depressurised and slider lock on, Section V-B2), visualized the key landmarks, and explored the very first section of the duodenum. Retroflexion (a technique where the camera of the endoscope is turned back onto itself to view the area around the insertion tube) was then performed in the gastric body. This maneuver was accomplished with the DCE through a technique similar to that used in conventional endoscopy - the endoscope tip was maximally deflected and the insertion tube was then gently advanced to bank-it off the compliant gastric wall. Fig. 12(b) shows the ET motion inside the anatomy as visualized by the conventional FE, while Fig. 12(c) shows a view of the DCE. Illumination and image quality of the DCE were considered acceptable by the gastroenterologist. In terms of procedure duration, the visualization of the anatomical key landmarks was performed with the conventional FE in 20s, while 51s were necessary with the DCE.

The expert user highly appreciated the light weight (675 g) and the portability (on-board battery and light source, and Wi-Fi video transmission to smartphone or tablet) of the DCE. The possibility to stream the endoscopic video to any smart device was noted as a benefit for widespread adoption of this technology outside the endoscopy suite. Time to set up the DCE from taking it out of its case to starting the procedure was below 3 minutes.

VII. DISCUSSION

This paper presents an innovative UGI endoscope that is easy to set up, easy to use, extremely portable, and that can to be manufactured at an ultra-low cost.

Through coupling of a multi-backbone UI and a soft PBA-based ET, we presented a device that leverages the precision of multi-backbone continuum manipulators, with the compliance of soft robots. The adaptation of standard associated modeling techniques, presented in Section IV, demonstrated a method for realizing device designs that can deliver user-to-task mapping at a tunable scale.

With respect to the requirements described in Section II, the device at the current prototyping stage: has a linear relationship between output bending angle of the ET (Θ_v) and input bending angle of the UI (Θ_u) from $0°$ to $65°$, on bending planes δ_v spanning from $0°$ to $360°$; minimizes the risk of perforation thanks to an estimated flexural strength six times lower than conventional FE; has an ET 13.5 mm in diameter, and a 7 mm insertion tube; allows for the visualization of relevant anatomical landmarks within a time comparable with conventional EGD; achieves bending error ($5.35° \pm 3.17°$) lower than what has been reported for clinically used FE [37]; is extremely easy to transport and set up; is composed of a disposable endoscopic probe with material cost below 10 USD.

The main limitations of DCE compared to FE are a limited workspace, and a larger diameter. These are due to the use of off-the-shelf rubber bellows that were chosen to assess the feasibility of the design, and develop analytical models for characterizing user-to-task mappings. Future design iterations will use custom bellows with smaller diameter and larger range of motion to decrease the ET diameter, and hence enable unsedated procedures, and facilitate retroflexion. Further studies will be conducted to quantify the achievable range of the user-to-task mapping to match the steering preference of end users.

Although the results of the usability and preclinical trials are promising in terms of efficacy and usability, the presented study is limited in the number of participants and quantitative findings. Thus, larger trials with metrics for ease-of-use and learning curve assessments of the DCE should be performed.

Critically, a solution that enables DCE operation with one hand (e.g. a wearable device handle with a smaller UI, or a larger UI that can be pivoted on a surface such as the examination bed) should be explored to facilitate further DCE use.

The current version of the device is solely for diagnostic procedures, i.e. it does not have a therapeutic channel. Limited stiffness of the current PBA does not allow passing a tool to the tip; however, the insufflation channel at the base of the PBA can be modified for delivering tools. Through coupling a modified version of the device with a steerable biopsy tool, such as the one proposed by [52], or with more specific tool such as a cryogenic balloon for treatment of Barrett's esophagus [53], the DCE may be enabled to perform biopsy or therapeutic procedures.

VIII. CONCLUSION

The proposed DCE has the potential to provide untrained personnel (e.g. GP, ER/ICU clinicians) with a simple to use, low-cost, and hygienic endoscopic solution for triage and diagnosis of upper GI tract pathology in non-traditional endoscopic settings. Furthermore, the analytical modeling techniques pre-

sented may facilitate adaptation of future DCE designs that could improve usability, functionality and further reduce costs.

Through adoption of DCE based platforms, the issues associated with costly, non-intuitive conventional FEs may be mitigated, and, by moving to a disposable endoscope, cross contamination may be prevented. In combination, the benefits of DCEs may allow for more widespread implementation of UGI tract screening, ultimately reducing mortality associated with disease of the UGI tract.

REFERENCES

[1] A. F. Peery, E. S. Dellon, J. Lund, S. D. Crockett, C. E. McGowan, W. J. Bulsiewicz, L. M. Gangarosa, M. T. Thiny, K. Stizenberg, D. R. Morgan *et al.*, "Burden of gastrointestinal disease in the united states: 2012 update," *Gastroenterology*, vol. 143, no. 5, pp. 1179–1187, 2012.
[2] MedlinePlus. (2018, Jul) Egd - esophagogastroduodenoscopy. [Online]. Available: https://medlineplus.gov/ency/article/003888.htm
[3] E. Rozeboom, J. Ruiter, M. Franken, and I. Broeders, "Intuitive user interfaces increase efficiency in endoscope tip control," *Surgical Endoscopy*, vol. 28, no. 9, pp. 2600–2605, 2014.
[4] J. Kovaleva, F. T. Peters, H. C. Van Der Mei, and J. E. Degener, "Transmission of infection by flexible gastrointestinal endoscopy and bronchoscopy," *Clinical Microbiology Reviews*, vol. 26, no. 2, pp. 231–254, 2013.
[5] P. Murray, "Preventable tragedies: Superbugs and how ineffective monitoring of medical device safety fails patients," *United States: United States Senate Health, Education, Labor and Pensions Committee*, 2016.
[6] C. L. Ofstead, M. R. Quick, J. E. Eiland, and S. J. Adams, "A glimpse at the true cost of reprocessing endoscopes," *International Association of Healthcare Central Service Material Management*, 2017.
[7] M. Broe, M. Barry, S. Patchett, and A. Hill, "Evaluating the clinical efficacy and cost effectiveness of direct access endoscopy," *The Surgeon*, vol. 11, no. 6, pp. 304–308, 2013.
[8] J. G. Lee, S. Turnipseed, P. S. Romano, H. Vigil, R. Azari, N. Melnikoff, R. Hsu, D. Kirk, P. Sokolove, and J. W. Leung, "Endoscopy-based triage significantly reduces hospitalization rates and costs of treating upper gi bleeding: a randomized controlled trial," *Gastrointestinal endoscopy*, vol. 50, no. 6, pp. 755–761, 1999.
[9] J. Ferlay, I. Soerjomataram, R. Dikshit, S. Eser, C. Mathers, M. Rebelo, D. M. Parkin, D. Forman, and F. Bray, "Cancer incidence and mortality worldwide: sources, methods and major patterns in globocan 2012," *International Journal of Cancer*, vol. 136, no. 5, pp. E359–E386, 2015.
[10] W. Chen, R. Zheng, P. D. Baade, S. Zhang, H. Zeng, F. Bray, A. Jemal, X. Q. Yu, and J. He, "Cancer statistics in china, 2015," *CA: a Cancer Journal for Clinicians*, vol. 66, no. 2, pp. 115–132, 2016.
[11] T. Rösch, A. Adler, H. Pohl, E. Wettschureck, M. Koch, B. Wiedenmann, and N. Hoepffner, "A motor-driven single-use colonoscope controlled with a hand-held device: a feasibility study in volunteers," *Gastrointestinal Endoscopy*, vol. 67, no. 7, pp. 1139–1146, 2008.
[12] Z. Liao, X. Hou, E.-Q. Lin-Hu, J.-Q. Sheng, Z.-Z. Ge, B. Jiang, X.-H. Hou, J.-Y. Liu, Z. Li, Q.-Y. Huang *et al.*, "Accuracy of magnetically controlled capsule endoscopy, compared with conventional gastroscopy, in detection of gastric diseases," *Clinical Gastroenterology and Hepatology*, vol. 14, no. 9, pp. 1266–1273, 2016.

[13] F. Campisano, F. Gramuglia, I. R. Dawson, C. T. Lyne, M. L. Izmaylov, S. Misra, E. De Momi, D. R. Morgan, K. L. Obstein, and P. Valdastri, "Gastric cancer screening in low-income countries: System design, fabrication, and analysis for an ultralow-cost endoscopy procedure," *IEEE Robotics & Automation Magazine*, vol. 24, no. 2, pp. 73–81, 2017.

[14] J. Burgner-Kahrs, D. C. Rucker, and H. Choset, "Continuum robots for medical applications: A survey," *IEEE Transactions on Robotics*, vol. 31, no. 6, pp. 1261–1280, 2015.

[15] A. Orekhov, C. Abah, and N. Simaan, "Snake-like robots for minimally invasive, single-port, and intraluminal surgeries," in *The Encyclopedia of Medical Robotics*. World Scientific, 2018, ch. 8, pp. 203–243.

[16] P. Sears and P. Dupont, "A steerable needle technology using curved concentric tubes," in *Intelligent Robots and Systems, 2006 IEEE/RSJ International Conference on*. IEEE, 2006, pp. 2850–2856.

[17] R. J. Webster, A. M. Okamura, and N. J. Cowan, "Toward active cannulas: Miniature snake-like surgical robots," in *Intelligent Robots and Systems, 2006 IEEE/RSJ International Conference on*. IEEE, 2006, pp. 2857–2863.

[18] N. Simaan, "Snake-like units using flexible backbones and actuation redundancy for enhanced miniaturization," in *Robotics and Automation, 2005 IEEE/ICRA International Conference on*. IEEE, 2005, pp. 3012–3017.

[19] R. E. Goldman, A. Bajo, L. S. MacLachlan, R. Pickens, S. D. Herrell, and N. Simaan, "Design and performance evaluation of a minimally invasive telerobotic platform for transurethral surveillance and intervention," *IEEE Transactions on Biomedical Engineering*, vol. 60, no. 4, pp. 918–925, 2013.

[20] N. Simaan, K. Xu, W. Wei, A. Kapoor, P. Kazanzides, R. Taylor, and P. Flint, "Design and integration of a telerobotic system for minimally invasive surgery of the throat," *The International Journal of Robotics Research*, vol. 28, no. 9, pp. 1134–1153, 2009.

[21] N. Simaan, A. Bajo, A. Reiter, L. Wang, P. Allen, and D. Fowler, "Lessons learned using the insertable robotic effector platform (irep) for single port access surgery," *Journal of Robotic Surgery*, vol. 7, no. 3, pp. 235–240, 2013.

[22] J. H. Kaouk, G.-P. Haber, R. Autorino, S. Crouzet, A. Ouzzane, V. Flamand, and A. Villers, "A novel robotic system for single-port urologic surgery: first clinical investigation," *European Urology*, vol. 66, no. 6, pp. 1033–1043, 2014.

[23] K. Xu, J. Zhao, and M. Fu, "Development of the sjtu unfoldable robotic system (surs) for single port laparoscopy," *IEEE/ASME Transactions on Mechatronics*, vol. 20, no. 5, pp. 2133–2145, 2015.

[24] P. Dario, M. C. Carrozza, M. Marcacci, S. D'Attanasio, B. Magnami, O. Tonet, and G. Megali, "A novel mechatronic tool for computer-assisted arthroscopy," *IEEE Transactions on Information Technology in Biomedicine*, vol. 4, no. 1, pp. 15–29, 2000.

[25] R. E. Goldman, A. Bajo, and N. Simaan, "Compliant motion control for multisegment continuum robots with actuation force sensing," *IEEE Transactions on Robotics*, vol. 30, no. 4, pp. 890–902, 2014.

[26] M. Cianchetti, C. Laschi, A. Menciassi, and P. Dario, "Biomedical applications of soft robotics," *Nature Reviews Materials*, vol. 3, p. 143153, 2018.

[27] R. V. Martinez, J. L. Branch, C. R. Fish, L. Jin, R. F. Shepherd, R. M. Nunes, Z. Suo, and G. M. Whitesides, "Robotic tentacles with three-dimensional mobility based on flexible elastomers," *Advanced Materials*, vol. 25, no. 2, pp. 205–212, 2013.

[28] M. Cianchetti, T. Ranzani, G. Gerboni, T. Nanayakkara, K. Althoefer, P. Dasgupta, and A. Menciassi, "Soft robotics technologies to address shortcomings in today's minimally invasive surgery: the stiff-flop approach," *Soft Robotics*, vol. 1, no. 2, pp. 122–131, 2014.

[29] H. Abidi, G. Gerboni, M. Brancadoro, J Fras, A. Diodato, M. Cianchetti, H. Wurdemann, K. Althoefer, and A. Menciassi, "Highly dexterous 2-module soft robot for intra-organ navigation in minimally invasive surgery," *The International Journal of Medical Robotics and Computer Assisted Surgery*, vol. 14, no. 1, p. e1875, 2018.

[30] Y. Bailly and Y. Amirat, "Modeling and control of a hybrid continuum active catheter for aortic aneurysm treatment," in *Robotics and Automation, 2005 IEEE/ICRA International Conference on*. IEEE, 2005, pp. 924–929.

[31] D. O'Brien and D. M. Lane, "3d force control system design for a hydraulic parallel bellows continuum actuator," in *Robotics and Automation, 2001 IEEE/ICRA International Conference on*, vol. 3. IEEE, 2001, pp. 2375–2380.

[32] T. Gagarina and P. Joli, "Modeling and experimental analysis of a new bellow type actuators for active catheter end-effector," in *Robot and Human Interactive Communication, 2001 10th IEEE International Workshop on*. IEEE, 2001, pp. 612–617.

[33] V. Falkenhahn, A. Hildebrandt, R. Neumann, and O. Sawodny, "Dynamic control of the bionic handling assistant," *IEEE/ASME Transactions on Mechatronics*, vol. 22, no. 1, pp. 6–17, 2017.

[34] T. Mahl, A. Hildebrandt, and O. Sawodny, "A variable curvature continuum kinematics for kinematic control of the bionic handling assistant," *IEEE Transactions on Robotics*, vol. 30, no. 4, pp. 935–949, 2014.

[35] N. Garbin, L. Wang, J. H. Chandler, K. L. Obstein, N. Simaan, and P. Valdastri, "A disposable continuum endoscope using piston-driven parallel bellow actuator," in *Medical Robotics (ISMR), 2018 International Symposium on*. IEEE, 2018, pp. 1–6.

[36] H. H. Hopkins and N. S. Kapany, "A flexible fibrescope, using static scanning," *Nature*, vol. 173, no. 4392, p. 39, 1954.

[37] E. D. Rozeboom, R. Reilink, M. P. Schwartz, P. Fockens, and I. A. Broeders, "Evaluation of the tip-bending response in clinically used endoscopes," *Endoscopy international open*, vol. 4, no. 4, p. E466, 2016.

[38] J. Wehrmeyer, J. Barthel, J. Roth, and T. Saifuddin, "Colonoscope flexural rigidity measurement," *Medical and Biological Engineering and Computing*, vol. 36, no. 4, pp. 475–479, 1998.

[39] G. M. Eisen, T. H. Baron, J. A. Dominitz, D. O. Faigel, J. L. Goldstein, J. F. Johanson, J. S. Mallery, H. M. Raddawi, J. J. Vargo II, J. P. Waring *et al.*, "Complications of upper gi endoscopy," *Gastrointestinal endoscopy*, vol. 55, no. 7, pp. 784–793, 2002.

[40] L. Trevisani, V. Cifalà, S. Sartori, G. Gilli, G. Matarese, and V. Abbasciano, "Unsedated ultrathin upper endoscopy is better than conventional endoscopy in routine outpatient gastroenterology practice: a randomized trial," *World Journal of Gastroenterology: WJG*, vol. 13, no. 6, pp. 906–911, 2007.

[41] R. T. Garcia, J. P. Cello, M. H. Nguyen, S. J. Rogers, A. Rodas, H. N. Trinh, N. H. Stollman, G. Schlueck, and K. R. McQuaid, "Unsedated ultrathin egd is well accepted when compared with conventional sedated egd: a multicenter randomized trial," *Gastroenterology*, vol. 125, no. 6, pp. 1606–1612, 2003.

[42] J. M. Inadomi, C. L. Gunnarsson, J. A. Rizzo, and H. Fang, "Projected increased growth rate of anesthesia professional–delivered sedation for colonoscopy and egd in the united states: 2009 to 2015," *Gastrointestinal Endoscopy*, vol. 72, no. 3, pp. 580–586, 2010.

[43] M. Ferrua and R. Singh, "Modeling the fluid dynamics in a human stomach to gain insight of food digestion," *Journal of food science*, vol. 75, no. 7, pp. R151–R162, 2010.

[44] G. Harvin, "Review of musculoskeletal injuries and prevention in the endoscopy practitioner," *Journal of Clinical Gastroenterology*, vol. 48, no. 7, pp. 590–594, 2014.

[45] O. W. Cass, M. L. Freeman, C. J. Peine, R. T. Zera, and G. R. Onstad, "Objective evaluation of endoscopy skills during training," *Annals of Internal Medicine*, vol. 118, no. 1, pp. 40–44, 1993.

[46] T. D. Nguyen and J. Burgner-Kahrs, "A tendon-driven continuum robot with extensible sections," in *Intelligent Robots and Systems, 2015 IEEE/RSJ International Conference on*. IEEE, 2015, pp. 2130–2135.

[47] A. D. Kapadia and I. D. Walker, "Self-motion analysis of extensible continuum manipulators," in *Robotics and Automation, 2013 IEEE/ICRA International Conference on*. IEEE, 2013, pp. 1988–1994.

[48] K. Xu and N. Simaan, "Actuation compensation for flexible surgical snake-like robots with redundant remote actuation," in *Robotics and Automation, 2006 IEEE/ICRA International Conference on*. IEEE, 2006, pp. 4148–4154.

[49] R. Roy, L. Wang, and N. Simaan, "Modeling and estimation of friction, extension, and coupling effects in multisegment continuum robots," *IEEE/ASME Transactions on Mechatronics*, vol. 22, no. 2, pp. 909–920, 2017.

[50] C. Medical. (2018, May) Single-use self-propelled colonoscope. [Online]. Available: https://consis-medical.com/

[51] N. Garbin, S. Sarker, D. C. Sohn, P. R. Slawinski, P. Valdastri, and K. L. Obstein, "Su1180 evaluation of a novel disposable upper endoscope for unsedated bedside (non-endoscopy unit based) assessment of the upper gastrointestinal (ugi) tract," *Gastrointestinal Endoscopy*, vol. 85, no. 5, p. AB304, 2017.

[52] K. Oliver-Butler, Z. H. Epps, and D. C. Rucker, "Concentric agonist-antagonist robots for minimally invasive surgeries," in *Medical Imaging 2017: Image-Guided Procedures, Robotic Interventions, and Modeling*, vol. 10135. International Society for Optics and Photonics, 2017, pp. 10 135 111–8.

[53] D. W. Schölvinck, H. T. Künzli, C. Kestens, P. D. Siersema, F. P. Vleggaar, M. I. Canto, H. Cosby, J. A. Abrams, C. J. Lightdale, E. Tejeda-Ramirez *et al.*, "Treatment of barrett's esophagus with a novel focal cryoablation device: a safety and feasibility study," *Endoscopy*, vol. 47, no. 12, pp. 1106–1112, 2015.